JGR Oceans

RESEARCH ARTICLE
10.1029/2021JC018023

Wind-Induced Hypolimnetic Upwelling Between the Multi-Depth Basins of Lake Geneva During Winter: An Overlooked Deepwater Renewal Mechanism?

Rafael S. Reiss[1], U. Lemmin[1], and D. A. Barry[1]

[1]Ecological Engineering Laboratory (ECOL), Institute of Environmental Engineering (IIE), Faculty of Architecture, Civil and Environmental Engineering (ENAC), Ecole Polytechnique Fédérale de Lausanne (EPFL), Lausanne, Switzerland

Key Points:

- Complex dynamics of upwelling between two basins of a large lake are revealed for the first time by field observations and 3D modeling
- Frequent, strong along-axis winds generate upwelling of deep hypolimnetic waters from the deep basin into the shallow basin
- Upwelled deep waters descend back to great depths after mixing with fresher waters of the shallow basin, contributing to deepwater renewal

Supporting Information:

Supporting Information may be found in the online version of this article.

Correspondence to:

R. S. Reiss,
rafael.reiss@epfl.ch

Citation:

Reiss, R. S., Lemmin, U., & Barry, D. A. (2022). Wind-induced hypolimnetic upwelling between the multi-depth basins of Lake Geneva during winter: An overlooked deepwater renewal mechanism? *Journal of Geophysical Research: Oceans*, *127*, e2021JC018023. https://doi.org/10.1029/2021JC018023

Received 22 SEP 2021
Accepted 14 MAY 2022

Abstract Combining field observations, 3D hydrodynamic modeling, and particle tracking, we investigated wind-induced interbasin exchange between the *Petit Lac* (*PL*) (depth 75 m) and *Grand Lac* (*GL*) (depth 309 m) basins of Lake Geneva in early winter. Following a strong 2.5-day wind event, a two-layer flow field developed, where the downwind surface drift into the *GL* was balanced by counterflowing hypolimnetic currents into the *PL*. Velocities in both layers exceeded 20 cm s^{-1}, with the highest values (27 cm s^{-1}) found near the bottom. For 3.5 days, hypolimnetic temperatures at the confluence decreased to values found in the deep *GL* hypolimnion at 180-m depth. Approximately 1.5 days after the wind event ceased, currents reversed and upwelled waters returned into the deep *GL* hypolimnion. The Coriolis force strongly modified the interbasin exchange dynamics, which were well represented by the model. Particle tracking revealed a "current loop," that is, water from below 150-m depth first upwelled into the *PL*, intruded approximately 10 km (half its length), and then descended back into the *GL* hypolimnion. Model results showed that the *PL* hypolimnetic volume doubled during the upwelling. Low model-based gradient Richardson numbers and temperature inversions in CTD profiles indicated turbulent mixing between the upwelled *GL* and surrounding *PL* waters. Our findings demonstrate that hypolimnetic upwelling between the two basins frequently occurs during winter and could potentially be an important, but as yet overlooked mechanism for hypolimnetic-epilimnetic exchange and deepwater renewal in Lake Geneva, and probably in other multi-depth basin lakes under similar wind conditions.

Plain Language Summary Deepwater Renewal (DR) is essential for maintaining a healthy lake ecosystem. Top-to-bottom convective cooling and the consequent mixing and DR are, however, expected to weaken due to climate change and milder winters. Therefore, a good understanding of alternative DR processes is crucial, yet is lacking at present. As a potential alternative DR process, we investigated wind-induced interbasin exchange between the two basins (max. depths 75 and 309 m) of weakly stratified Lake Geneva, Western Europe's largest lake, during winter. Combining field observations, 3D hydrodynamic modeling and particle tracking, we show for the first time that during this process waters from as deep as ∼150–200 m and as far away as 25 km are drawn into the small shallow basin for several days. They can intrude up to ∼10 km into the shallow basin, doubling its hypolimnion volume, and mix intensively with the oxygen-rich ambient waters, before draining back into the deep layers of the large deep basin. This process frequently occurs during early winter in Lake Geneva and probably in other deep multi-basin lakes under similar conditions. These findings should be taken into consideration when establishing long-term predictions of lake system dynamics related to climate change.

1. Introduction

The exchange flow between distinct sub-basins and large embayments is a ubiquitous feature of many lakes, for example, Lake Huron (Bennett, 1988; Nguyen et al., 2014), Lake Erie (Bartish, 1987; Jabbari et al., 2019, 2021; Niu et al., 2015), Lake Simcoe (Flood et al., 2020; Nürnberg et al., 2013), Lake Constance (Appt et al., 2004; Kocsis et al., 1998), and Lake Geneva (Cimatoribus et al., 2019; Umlauf & Lemmin, 2005). Horizontal gradients in water quality between basins can result from a number of processes. For example, different seasonal mixing regimes between basins with different depths can produce biochemical gradients between their hypolimnia (e.g., Lake Geneva: CIPEL, 2016; Lake Garda: Salmaso, 2005). The thin and usually warmer hypolimnion of a shallow basin is prone to earlier oxygen depletion compared to the larger, colder hypolimnion of an adjacent deep basin (e.g., Ahrnsbrak & Wing, 1998; Cornett & Rigler, 1979; Scavia et al., 2014). Consequently, interbasin exchange

can be an important transport process with potentially significant ecological consequences, both locally and basin-wide.

Interbasin exchange is caused by diverse processes. Density-driven exchange not only can result from differential heating (Monismith et al., 1990; Wells & Sealock, 2009) or cooling (Monismith et al., 1990; Okubo, 1995; Oonishi, 1995) of adjacent basins with different depths, but also from geochemical gradients between basins due to river inflow and/or differential vertical mixing due to non-uniform wind fields (Aeschbach-Hertig et al., 1996). In stratified systems, wind stress can act indirectly through internal wave pumping between basins (e.g., van Senden and Imboden, 1989) or directly via two-way advective exchange, whereby a downwind surface drift toward one basin is balanced by a subsurface counterflow toward the other basin (Boyce et al., 1980; Laval et al., 2008).

The importance of wind-driven coastal upwelling in lakes, due to its role in nutrient cycling, deepwater renewal, and vertical and horizontal exchange, is well recognized. It has been documented, both in small lakes where rotational effects are negligible (e.g., Coman & Wells, 2012; Pöschke et al., 2015), and in large lakes where the upwelling dynamics are modified by the Coriolis force (for a discussion see, e.g., Amadori et al., 2020 and Roberts et al., 2021). In the latter case, in addition to generating upwind upwelling in the direction of the wind, alongshore wind stress produces cross-shore Ekman transport in the upper layers. Depending on the wind direction, this results in a nearshore divergence (convergence) in the upper layers that is compensated for by coastal upwelling of deep waters (coastal downwelling of surface waters) perpendicular to the wind (e.g., Amadori et al., 2020, 2018; Piccolroaz et al., 2019; Rao & Murthy, 2001; Reiss et al., 2020).

Interbasin exchange caused by internal waves has received considerable attention in the context of horizontal exchange flows between basins and the flushing of side basins (e.g., Flood et al., 2020; Lawrence et al., 1997). Horizontal exchange between the two basins of Lake Geneva resulting from internal Kelvin wave propagation was investigated by Umlauf and Lemmin (2005). Although this process can flush the shallow western basin's hypolimnion (maximum depth 75 m), it does not significantly contribute to the renewal of the deep waters in the *Grand Lac* basin (maximum depth 309 m). On the other hand, direct wind-driven interbasin exchange in large lakes, in particular vertical exchange and hypolimnetic upwelling between basins of different depths, is less studied, with the exception of shallow Lake Erie, where most field efforts date back several decades (e.g., Boyce et al., 1980; Saylor & Miller, 1987), as summarized in the review by Bartish (1987). However, with increasing global warming and the consequent weakening of convective cooling (e.g., Goldman et al., 2013), the potential of such an alternative deepwater renewal process needs to be addressed.

In the present study, we therefore investigated interbasin exchange during a typical, strong wind event in weakly stratified Lake Geneva during early winter, focusing on the as yet little-known dynamics of the vertical exchange between its shallow (*Petit Lac*, max. depth 75 m) and its deep (*Grand Lac*, max. depth 309 m) basins, based on extensive field observations, three-dimensional (3D) hydrodynamic modeling, and model-based Lagrangian particle tracking. The following questions are addressed:

1. What are the prevailing current patterns during wind-induced interbasin exchange and are they affected by the Coriolis force?
2. Does this transport process produce deepwater upwelling from the deep *Grand Lac* into the shallow *Petit Lac* basin? If so, how far does the upwelled water penetrate into the *Petit Lac* basin, how much of the *Petit Lac* volume is affected, and what happens to the upwelled waters after the wind event?
3. Can such an upwelling between the two basins provide a potentially significant mechanism for hypolimnetic-epilimnetic exchange and deepwater renewal?
4. Does the Coriolis force affect the flow of the upwelled water masses in the *Petit Lac*? If so, can it cause coastal upwelling, and what is the role of the topography?

Since the phenomenon investigated here is an interbasin exchange flow combined with topographic and coastal upwelling, it will hereinafter be referred to as “interbasin upwelling.”

Additional clarifications and details on certain topics mentioned in the text are provided in Supporting Information S1 section with figures and tables denoted with prefix S.

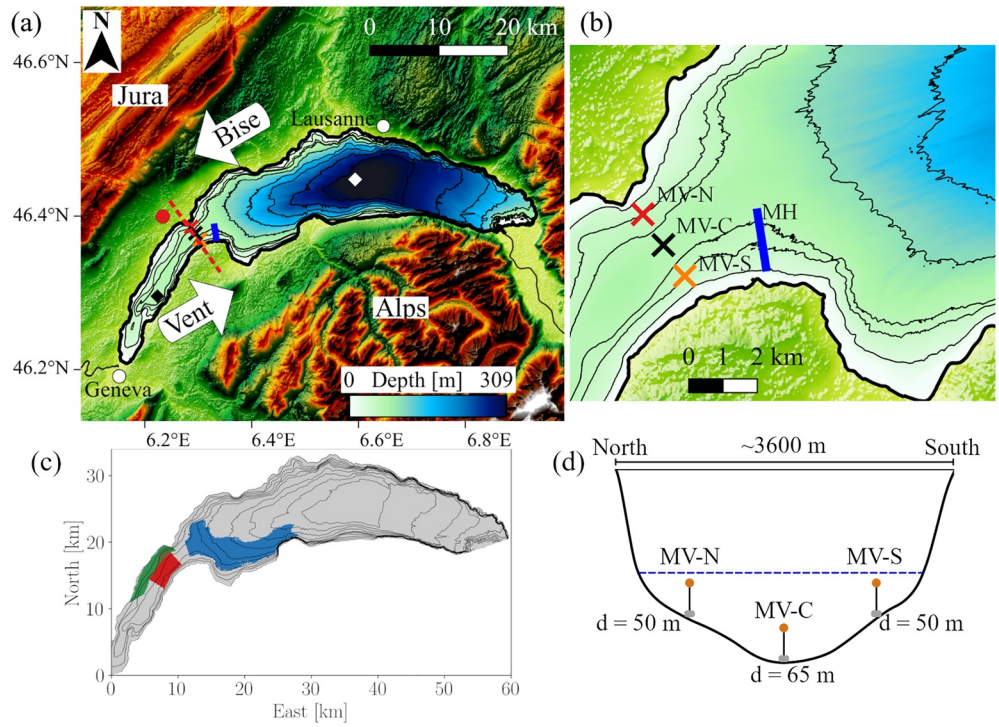

Figure 1. (a) Map of Lake Geneva including the surrounding topography. The red dashed line (confluence) delimits the small *Petit Lac* and the large *Grand Lac* basins. Two strong winds, namely the *Vent* from the southwest and the *Bise* from the northeast blow over most of the lake. Full-depth temperature profiles are taken at CIPEL stations SHL2 (white diamond; depth 309 m) and GE3 (black diamond; depth 71 m). Meteorological data were recorded at the MeteoSwiss Nyon station (red circle). Depth is given by the colorbar and the isobath contours (0, 25, 50, 60, 100, 150, 200, 250, and 300 m). (b) Close-up of the confluence area, with the moorings, MV-N (red cross), MV-C (black cross), MV-S (orange cross), and MH (blue line), deployed during winter 2018–2019. Isobath contours (0, 25, 50, 60, 100, and 150 m) are given. (c) Regions where particles were released during the particle tracking simulations: B (red), S (green) in the *Petit Lac*, and L (blue) in the *Grand Lac* (see Section 2.4 for details). (d) Depth-exaggerated schematic view of the 10-m long vertical moorings MV-N, MV-C, and MV-S, deployed at the confluence. The horizontal blue dashed line indicates the thermocline depth before the wind started.

2. Material and Methods

2.1. Study Site

Lake Geneva (local name: *Lac Léman*) is a large monomictic lake located between France and Switzerland. With a surface area of 580 km^2, a total length of ~73 km, and a volume of ~89 km^3, Lake Geneva is Western Europe's largest lake. It is crescent-shaped and consists of two basins: a small western basin, called the *Petit Lac* (maximum depth 75 m, width 5 km, length 23 km) and a large eastern basin, called the *Grand Lac* (maximum depth 309 m and width 14 km; Figure 1a). The "confluence" of the two basins is ~3.5 km wide (Figure 1b). River throughflow is small, resulting in a flushing time (also referred to as theoretical residence time; Monsen et al., 2002) of ~11 years (CIPEL, 2019).

The shallow *Petit Lac* undergoes complete vertical mixing every winter, usually in late December or early January. In contrast, in the deep *Grand Lac,* a weak thermocline, typically at ~100–150 m depth, remains throughout the cold season and full-depth convective overturning only occurs during severely cold winters (CIPEL, 2019). Although the latter has long been considered the only mechanism for deepwater renewal in Lake Geneva, recent studies suggest that 3D transport processes, such as differential cooling or wind-driven coastal upwelling, also play an important role (Lemmin, 2020; Reiss et al., 2020). Furthermore, due to its annual complete vertical mixing, water quality parameters, such as dissolved oxygen (higher values) and nutrient concentrations (lower values) in the *Petit Lac* differ considerably from those in the deep *Grand Lac* hypolimnion (e.g., CIPEL, 2016; Lavigne & Nirel, 2016). Therefore, hypolimnetic exchange between the two basins could have important effects on the lake's overall ecological state.

Coriolis force effects strongly modify the lake's hydrodynamics (e.g., Bauer et al., 1981; Bouffard & Lemmin, 2013; Cimatoribus et al., 2019, 2018; Lemmin, 2020; Lemmin et al., 2005; Lemmin & D'Adamo, 1996; Reiss et al., 2020). The inertial period is ∼16.5 hr.

Lake Geneva is surrounded by the Jura and Alp mountains, whose channeling effect creates two strong, dominant large-scale winds, namely the *Vent* from the southwest and the *Bise* from the northeast (Figure 1a), both approximately aligned with the main axis of the western half of the lake (see example for *Vent* in Figure S4 in Supporting Information S1). Both winds are characterized by a long fetch and high wind speeds (∼5–15 m s^{-1}) lasting for several days (e.g., Graf & Prost, 1980; Lemmin et al., 2005; Lemmin & D'Adamo, 1996) and generate most of the large-scale circulation in the lake (e.g., Bouffard & Lemmin, 2013; Lemmin et al., 2005; Reiss et al., 2020; Soulignac et al., 2021; Umlauf & Lemmin, 2005).

2.2. Field Observations

A field measurement campaign was conducted near the confluence between the *Petit Lac* and *Grand Lac* basins during winter 2018–2019 (Figure 1a). Three vertical moorings were deployed along the confluence: MV-C at 65-m depth, MV-N at 50 m, and MV-S at 50 m. MV-C was in the center, with MV-N ∼1 km to the northwest, and MV-S ∼ 1 km to the southeast (Figures 1b and 1d). Table S1 in Supporting Information S1 summarizes the mooring configurations, instrument settings, and deployment periods. Full-depth current profiles at all three moorings were recorded by bottom-mounted Teledyne RDI Workhorse Sentinel (300 kHz) acoustic Doppler current profilers (ADCPs). To investigate the interbasin exchange flow, current velocities were projected onto a vertical plane parallel to the isobaths at the confluence, that is, a plane rotated by ∼50° eastwards from the north (Figure 1b). Temperature profiles between 1 and 10 m above the lakebed were obtained from vertical lines equipped with 10 temperature loggers spaced at 1-m intervals. Near-bottom temperatures were measured every 80 m along a 1.5-km long horizontal thermistor line (mooring MH) equipped with 20 RBRsolo *T* temperature loggers, which was laid down on the lakebed perpendicular to the shoreline between 25- and 65-m depth (Figure 1b). To avoid the risk of burying by sediment deposition, the tips of the thermistors at MH were made slightly buoyant, so that the instruments stood vertically on the lakebed. In addition, conductivity temperature depth (CTD) casts were taken on 13 December 2018: (a) along a transect perpendicular to the shore near the confluence, and (b) along the central axis of the *Petit Lac*, starting at the confluence and intruding as far as 7 km into the *Petit Lac* basin (Figure S1 in Supporting Information S1).

The data sets were complemented by full-depth CTD profiles taken twice a month by the Commission Internationale pour la Protection des Eaux du Léman (CIPEL, last accessed on 3 June 2021; Rimet et al., 2020) at the deepest point of the *Grand Lac* (309 m; SHL2 in Figure 1a) and monthly at 70-m depth in the *Petit Lac* (GE3 in Figure 1a).

To complement the main data set from 2018 to 2019, two moorings were deployed in winter 2019–2020 at 100- and 150-m depth near the southern shore of the *Grand Lac* (Figure S12f in Supporting Information S1), both equipped with a down-looking Teledyne RDI Workhorse Sentinel (300 kHz) ADCP that measured the lowest ∼50 m of the water column (Table S1 in Supporting Information S1).

A meteorological station in Nyon, operated by the Swiss National Weather and Climate Service (MeteoSwiss; last accessed on 3 June 2021) and located onshore ∼5 km northwest of the study site, recorded wind speed and direction every 10 min (red circle in Figure 1a). Hourly moving averages were applied to the meteorological data prior to the analysis.

2.3. Hydrodynamic Model

We employed a hydrostatic version of the MITgcm code solving the 3D Boussinesq Navier-Stokes equations (Marshall et al., 1997). Originating from the oceanographic community, this code has successfully been applied to lakes (Djoumna et al., 2014; Dorostkar & Boegman, 2013; Dorostkar et al., 2017), and recently to Lake Geneva (Cimatoribus et al., 2018, 2019; Hamze-Ziabari et al., 2022; Reiss et al., 2020). The model employed free-slip conditions at the lateral boundaries and quadratic bottom drag. It was configured with a uniform horizontal Cartesian grid with a resolution of 113 m, 100 size-varying z-layers (30 cm at the surface, 2.8 and 4.8 m at the deepest points of the confluence and the *Grand Lac*, respectively) and a time step of 8 s. Except for the increased vertical

resolution to better resolve the bottom currents in both the *Petit Lac* and *Grand Lac*, the model configuration was similar to that used by Reiss et al. (2020) to investigate wind-driven coastal upwelling during winter in Lake Geneva. A detailed calibration of the model for Lake Geneva was carried out by Cimatoribus et al. (2018).

Realistic two-dimensional (2D) surface forcing was obtained from the COSMO-1 numerical weather model of MeteoSwiss at a 1.1-km resolution (Voudouri et al., 2017) and was linearly interpolated onto the MITgcm grid. The model was initialized with zero velocity and a horizontally homogenous temperature field derived from the temperature profile measured at SHL2 on 12 September 2018 at 15:00 (local time) (Figure S5 in Supporting Information S1) and run for 8 months. This starting date was chosen because the preceding days were calm, allowing the model to adjust to the initial conditions.

2.4. Particle Tracking

Lagrangian particle tracking based on the velocity output of the validated MITgcm model was used to analyze pathways of water masses. The code employed here was developed by Cimatoribus (2018) and is based on the algorithm described by Döös et al. (2013). It was recently applied to Lake Geneva to study: (a) the dispersion of riverine water from the lake's main tributary, the Rhône River (Cimatoribus et al., 2019), and (b) wind-driven coastal upwelling during winter at the northern shore of the *Grand Lac* basin (Reiss et al., 2020). Following Reiss et al. (2020), we used backward and forward particle tracking to determine the origin and fate of upwelled waters at different locations in the *Petit Lac*.

Three different particle tracking simulations, hereinafter referred to as simulations B (bottom), S (surface), and L (loop), were run to address aspects of the wind-driven circulation between the *Petit Lac* and *Grand Lac*. In each of the three simulations, a total of ∼200,000 to 300,000 particles were released, either simultaneously or at regular time intervals, as discussed below. The corresponding seeding regions are given in Figure 1c.

In simulation S, the coastal upwelling at the northern *Petit Lac* shore was investigated by releasing particles near the shore, in the upper 15 m of the water column at 1-m depth intervals (green area in Figure 1c). Simulation B addressed the hypolimnetic upwelling of deep *Grand Lac* water into the bottom layers of the *Petit Lac* by releasing particles in an approximately 3-km × 5-km wide area near the confluence at every vertical grid point below 40-m depth (red area in Figure 1c). For simulations B and S, the seeding regions, depths and times were determined based on the occurrence of low temperatures in the hydrodynamic simulations, indicating upwelling of hypolimnetic water (e.g., modeled surface temperatures in Figure 4a show the extent of the coastal upwelling in the *Petit Lac*, corresponding approximately to the area in which particles were released for simulation S, as illustrated in Figure 1c). Particles were released every 2 hr from 8 December at 12:00 to 10 December at 12:00 (simulation S) and from 8 December at 00:00 to 11 December at 00:00 (simulation B), and tracked both backward and forward in time. The seeding locations in simulation L were inferred from the backward tracking results of simulation B by selecting the origin locations of all particles originating from below 50-m depth within the *Grand Lac* (blue area in Figure 1c). In this case, ∼200,000 particles were released simultaneously on 7 December at 13:00 and forward tracked until 18 December at 00:00, thus describing the complete current loop, that is, the upwelling from deep regions within the *Grand Lac* into the *Petit Lac* and the subsequent descent back into the hypolimnion of the *Grand Lac*.

To determine the origin and fate of upwelled waters in different regions of the *Petit Lac*, the backward and forward trajectories of simulations S and B were classified by initial and final depths, respectively. Furthermore, the distance that upwelled *Grand Lac* water penetrated into the *Petit Lac,* hereinafter referred to as intrusion length, was determined by analyzing the trajectories of simulation L. This also allowed estimation of the time that upwelled *Grand Lac* water spent in the *Petit Lac* before descending back into the *Grand Lac* hypolimnion.

3. Results and Discussion

3.1. Field Observations

Temperatures recorded at mooring MV-C show that the *Petit Lac* remained weakly stratified until approximately 4 January 2019 (Figure S2 in Supporting Information S1). The thermocline depth before the interbasin upwelling event discussed in the following sections could not be determined from full-depth CIPEL temperature profiles at GE3 and SHL2 because the thermocline was strongly tilted between stations GE3 and SHL2 due to strong

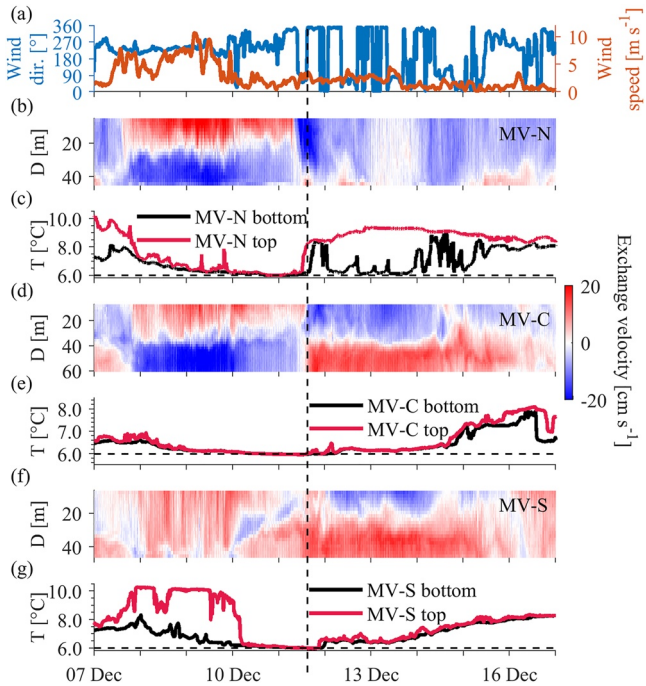

Figure 2. (a) Wind direction (blue) and speed (red) measured at the Nyon meteorological station. (b)–(g) Temperatures (T) and current velocities (vs. depth D) recorded at moorings MV-N (b), (c), MV-C (d), (e), and MV-S (f), (g), respectively. Current velocities are shown as "interbasin exchange velocities," that is, projected onto a vertical plane parallel to the isobaths at the confluence. The colorbar gives the velocity magnitude. Positive values indicate flow out of the *Petit Lac*. The horizontal dashed line in (c), (e), and (g) marks 6°C. The vertical dashed line indicates the transition from the upwelling to the relaxation phase. All dates refer to 2018. Note that vertical axes scales are different.

winds that preceded the closest sampling days. Instead, a thermocline depth of ~35 m in early December 2018 was inferred from the measurements at the horizontal thermistor line MH (Figure S3 in Supporting Information S1).

During the *Vent* event lasting from 7 to 10 December 2018, the overall mean wind speed measured at the Nyon meteorological station (Figure 1a) was ~5.5 m s^{-1} with hourly-averaged maximum values reaching 10.7 m s^{-1} (Figure 2a). The COSMO-1 data confirmed that the wind field over the lake was spatially relatively homogenous and aligned with the main axes of the *Petit Lac* and the western and central parts of the *Grand Lac* (Figure S4 in Supporting Information S1).

Current velocities and temperatures recorded at the vertical moorings, MV-S, MV-C, and MV-N, at the confluence of the two basins show that two phases (upwelling and relaxation) with distinctively different flow patterns can be identified (Figure 2), as discussed below.

3.1.1. Upwelling Phase: 7 December at ~19:00 to 11 December at ~10:00

Approximately half a day after the *Vent* wind started, a two-layer flow pattern was established at the central and northern moorings (MV-C, MV-N) and persisted for 1.5 days after the wind had ceased. The northeastward-directed wind stress caused strong epilimnetic flow from the *Petit Lac* into the *Grand Lac* (hereinafter referred to as outflow), balanced by a hypolimnetic counterflow from the *Grand Lac* into the *Petit Lac* (hereinafter referred to as inflow; Figure 2).

During this phase, *Grand Lac* water was continuously transported into the *Petit Lac* in a bottom current at the central and northern sections of the confluence. Inflowing current velocities near the bottom exceeded 27 cm s^{-1} at both MV-C and MV-N, with the corresponding temperatures gradually decreasing to below 6°C on 11 December around noon (Figures 2c and 2e). This suggests that the inflowing water originated from the deep *Grand Lac* hypolimnion. The lowest value of 5.96°C, measured 1 m above the lakebed at MV-C, corresponds to temperatures found at 180-m depth, as measured in the center of the *Grand Lac* basin at CIPEL station SHL2 in November and December 2018 (Figure S5 in Supporting Information S1). This was also the lowest temperature observed at the confluence during that winter.

The depth of the interface separating the in- and outflow varied between 25 and 35 m at MV-C, and 20 and 30 m at MV-N. At the latter mooring, this interface was observed generally at shallower depths, indicating that during the upwelling phase the thermocline was upwardly tilted at the northern shore (white color separating red and blue areas in Figure 2). This thermocline tilt, perpendicular to the wind stress, resembles a Coriolis force-driven Ekman-type coastal upwelling at the northern shore (e.g., Reiss et al., 2020) and is discussed in Section 3.3.2.

At the southern mooring (MV-S), a vertically relatively uniform outflow with velocities up to 16 cm s^{-1} prevailed. The corresponding near-bottom temperatures also dropped during the upwelling phase. However, the decrease was not continuous and lagged behind that of MV-N, indicating that it was not caused by direct deepwater upwelling at this location, but by the sporadic outflow of colder waters that had entered the *Petit Lac* north of MV-S. In contrast, the upper thermistors at this mooring showed increasing temperatures during the first 2 days of the upwelling. The maximum temperature of 10.27°C measured at the topmost thermistor (~40-m depth) on 8 December 01:20 is the same as that at the shallowest thermistor at MH, that is, at 25-m depth in the epilimnion. This temperature pattern can be explained by a Coriolis force-driven coastal downwelling of the thermocline at the southern shore during the upwelling phase, as confirmed by the 3D model and the horizontal thermistor line (Figure 4b and Figure S3 in Supporting Information S1).

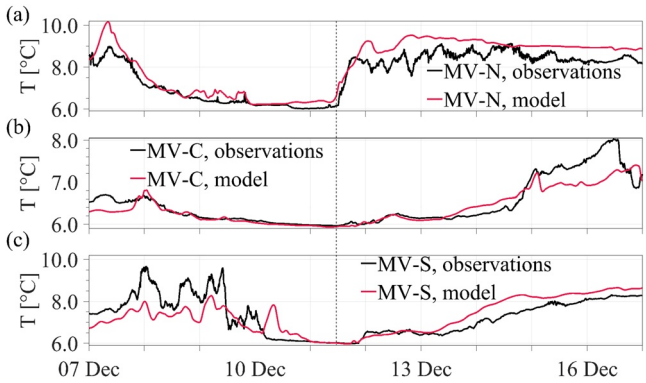

Figure 3. Depth-averaged temperatures in the lowest 10 m of the water column as observed (black) and modeled (red) from 7 to 17 December 2018 at moorings: (a) MV-N, (b) MV-C, and (c) MV-S. For mooring locations, see Figure 1b. All dates refer to 2018. The vertical dashed line indicates the transition from the upwelling phase to the relaxation phase.

3.1.2. Relaxation Phase: 11 December at ~14:00 to 15 December at ~14:00

Approximately 1.5 days after the wind had ceased, the flow pattern reversed at all moorings. The two-layer structure at MV-N was replaced by a uniform inflow over most of the water column, with only sporadic weak outflow near the lakebed. On the other hand, at MV-C, current directions reversed in both layers, resulting in an epilimnetic inflow and a hypolimnetic outflow. A similar two-layer structure was observed at MV-S with current velocities higher than during the upwelling phase, and outflowing velocities reaching 19 cm s^{-1}.

This period was characterized by a continuous, bottom-hugging outflow in the southern and central sections of the confluence. The depth of the interface separating the in- and outflow was not steady. More importantly, at MV-S, the interface appeared at shallower depths suggesting an upward tilt of the thermocline at the southern shore during the relaxation phase. This tilt was confirmed by north-south CTD casts at the confluence (Figure S1b in Supporting Information S1) and is further analyzed in Sections 3.2 and 3.3. The prevailing current patterns during both the upwelling and relaxation phases are summarized in Figures S6–S8 in Supporting Information S1. Temperatures increased during the relaxation phase at all moorings, in agreement with the flow field, indicating that the supply of deep, cold upwelled *Grand Lac* water had ceased (Figure 2).

The field observations demonstrated that the flow field during both phases of the interbasin upwelling was strongly affected by the Coriolis force, despite a horizontal distance between the northern and southern moorings of only ~2 km.

3.2. Model Results

The depth-averaged temperatures in the lowest 10 m of the water column as observed (black) and modeled (red) at the confluence from 7 to 17 December 2018 are compared in Figure 3. With root mean square errors (RMSEs) of 0.57°C, 0.26°C and 0.63°C at MV-N, MV-C and MV-S, respectively, the model captured well the characteristics of the two regimes: (a) the decreasing temperatures at the central and northern sections during the upwelling phase (Figures 3a and 3b), and (b) the gradually rising temperatures at the central and southern sections during the relaxation phase (Figures 3b and 3c).

Furthermore, the model well reproduced the currents during the two dynamic regimes characterized by: (a) a bottom inflow and surface outflow at the central and northern sections during the upwelling phase, and (b) a bottom outflow and surface inflow at the central and southern sections during the relaxation phase (Figures S6–S9 in Supporting Information S1).

The good performance of the hydrodynamic model allowed use of the model results to further investigate the complex 3D structure of the interbasin upwelling event. Vertical temperature and current velocity slices at selected locations as well as maps of the near-surface temperature anomalies at different times are displayed in Figure 4. Here, the near-surface temperature anomaly for each horizontal grid cell was computed as the difference between the local temperature and the basin-wide averaged temperature at 1.5-m depth.

The strong surface outflow and bottom inflow measured at the confluence during the upwelling phase prevailed in the entire *Petit Lac* basin, suggesting that upwelled cold *Grand Lac* water was transported far into the *Petit Lac* hypolimnion by a continuous southwestward current (Figure 4b and Figure S10a in Supporting Information S1). As a consequence, bottom temperatures at the confluence decreased continuously and the hypolimnion in the *Petit Lac* gradually thickened (Figure 4d). Based on the modeled 3D temperature field, the volume of the *Petit Lac* hypolimnion was estimated by taking the depth of the maximum Brunt-Väisälä frequency as its upper limit (Figures 5a and 5b). This analysis suggests that the volume of the *Petit Lac* hypolimnion had almost doubled by the end of the upwelling phase on 11 December at ~11:00 before again strongly decreasing during the relaxation phase (Figure 5c).

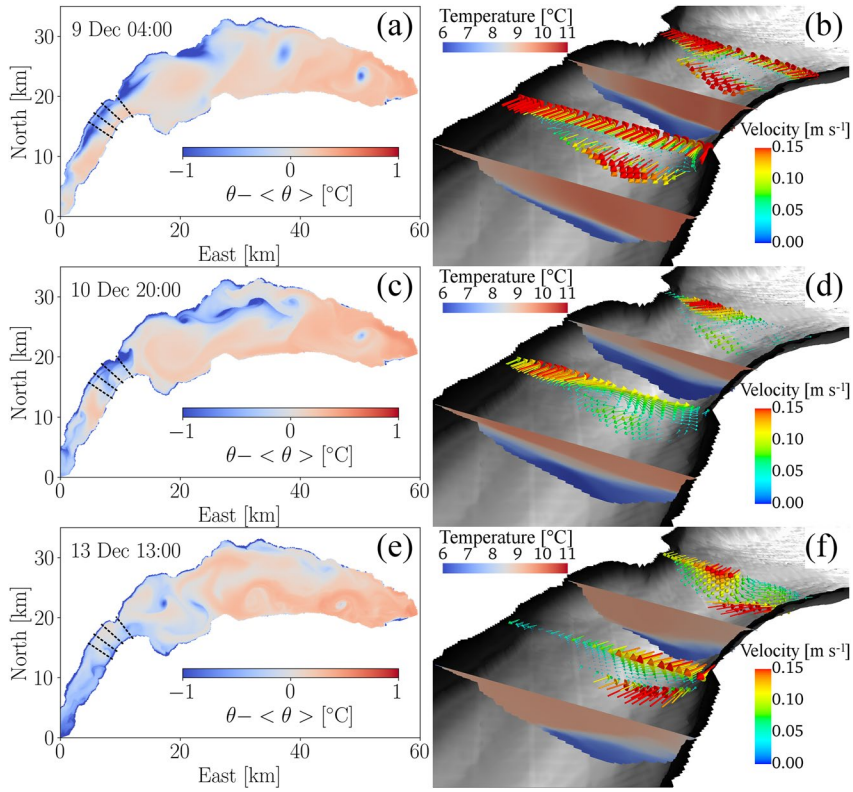

Figure 4. Modeled near-surface temperature anomaly at 1.5-m depth (a, c, e; see text for details) and current velocity and temperature slices at selected locations (b, d, f) at different times, that is, the maximum coastal upwelling in the *Petit Lac* basin (a), (b), 1 day after the wind stopped (c), (d), and the strongest outflowing bottom currents (e), (f). The colorbars give the surface temperature anomaly, temperature and current velocity, respectively. The locations of the vertical slices are marked in the surface contour plots by black dashed lines. The length of the velocity vectors is scaled with the magnitude of the velocity and, for clarity, not all vectors are shown.

Furthermore, the model results revealed an upward tilt of the thermocline at the northern shore perpendicular to the wind stress during the upwelling phase (Figures 4b and 4d), in agreement with the ADCP measurements at MV-C and MV-N (Figures 2b and 2d), confirming that the flow field was modified by the Coriolis force. At the same time, patches of cold water were detected along the northern *Petit Lac* shore, indicating a surfacing of the thermocline (Figure 4a). Although this temperature pattern resembles that of an Ekman-type coastal upwelling (e.g., Reiss et al., 2020), the underlying hydrodynamics appear to be different, as discussed in Section 3.3.2.

The current patterns reversed on 11 December around noon, signaling the start of the relaxation phase, and a northeastward hypolimnetic current was established in the entire *Petit Lac* (Figure 4f and Figure S10b in Supporting Information S1). During this period, *Grand Lac* waters that had previously upwelled into the *Petit Lac* flowed back into the *Grand Lac,* resulting in the thinning of the *Petit Lac* hypolimnion (Figure 4f). Furthermore, the volume estimation based on the Brunt-Väisälä frequency indicated that the *Petit Lac* hypolimnetic volume at the end of the relaxation phase was noticeably smaller than before the interbasin upwelling event (Figure 5c). This suggests that this process can efficiently flush most of the deep layers of the *Petit Lac* within only a few days. The highest current velocities, exceeding 20 cm s^{-1}, were found between 50 to 60-m depth near the confluence. The outflow then hugged the southern shore of the *Grand Lac* basin due to Coriolis deflection. Accordingly, the thermocline was tilted upward at the southern shore (Figure 4f), which was confirmed by north-south CTD transects taken across the confluence on 13 December around noon (Figure S1b in Supporting Information S1), as well as by the ADCP measurements at MV-C and MV-S (Figure 2).

The complete spatio-temporal evolution of the modeled temperatures and current velocities during both the upwelling and relaxation phases is shown in Movie S1.

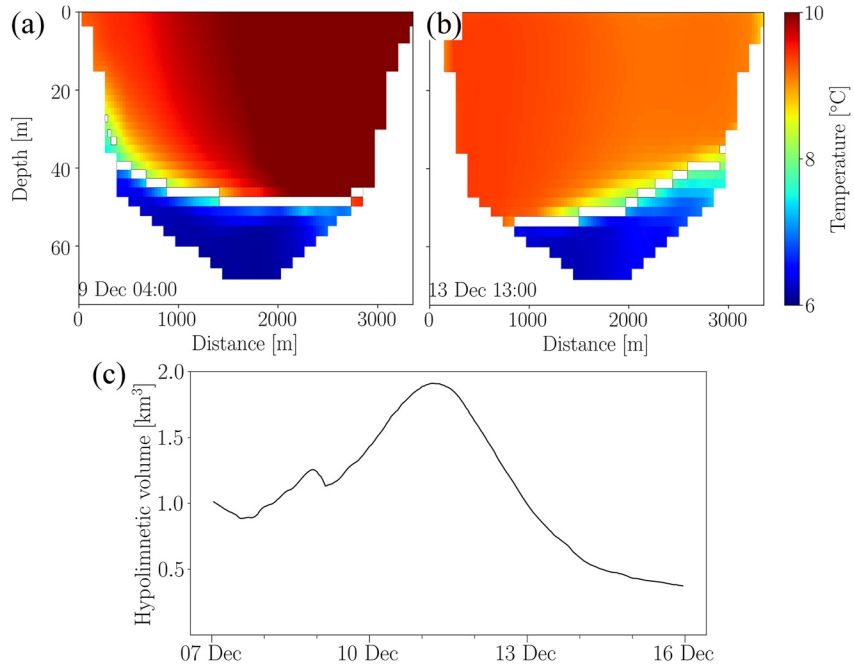

Figure 5. Modeled temperature at the confluence (red dashed line in Figure 1a) between the *Petit Lac* and *Grand Lac* basins: (a) during the upwelling phase (9 December 2018 at 04:00) and (b) during the relaxation phase (13 December 2018 at 13:00), respectively. Distance is given from the northern shore. The colorbar shows the temperature range. The overlaid white pixel lines in (a) and (b) mark the depth of the maximum buoyancy frequency for every profile along the transect. This depth was continuously determined in the entire *Petit Lac* basin and used to estimate the volume of its hypolimnion. (c) Time-series of the estimated volume of the *Petit Lac* hypolimnion (total volume of the *Petit Lac* is ~3 km^3).

3.3. Particle Tracking

During the interbasin upwelling event, hypolimnetic water from the deep *Grand Lac* was transported into the shallow *Petit Lac* (Figures 2 and 4). We investigated the pathways taken by the upwelled waters using backward and forward particle-tracking simulations at different sites. Particles were released in two seeding regions to investigate: (a) the upwelling into the hypolimnion of the *Petit Lac* (simulation B), and (b) the coastal upwelling at its northern shore (simulation S) (see Figure 1c for details). Doubling or tripling the number of particles by doubling the seeding frequency and increasing the vertical seeding resolution did not change the results of the particle tracking analysis, indicating their statistical robustness.

3.3.1. Hypolimnetic Upwelling Along the Bottom of the *Petit Lac*: The Current Loop

The backward and forward trajectories of the particles released during the upwelling phase in the *Petit Lac* hypolimnion (simulation B) are depicted in Figure 6. For better visualization, random subsets of ~2,500 (Figures 6a and 6c) and 10 particles (Figures 6b and 6d) are displayed. In agreement with the observed and modeled inflowing bottom currents at the confluence, the backward tracking revealed that particles, that is, water masses, were transported from the *Grand Lac* into the *Petit Lac* during this period. Furthermore, 44%, 25% and 6% of all particles originated from below 75, 100 and 150-m depths, respectively, confirming the deep origin of these waters, consistent with the low temperatures observed near the confluence bed (Figure 2). During the upwelling phase, the particle transport from the *Grand Lac* toward the confluence appeared to be concentrated in a bottom-hugging current following the southern shore, especially for particles originating from below 100-m depth (Figures 6a and 6b). This current structure, that is, the strong bottom current directed toward the *Petit Lac*, was confirmed by moored ADCP measurements near the southern shore of the *Grand Lac* during a similar interbasin upwelling event in December 2019 (Figure S12 in Supporting Information S1).

Further insight into the origin of the upwelled waters was gained by grouping the particles of backward tracking simulation B according to their seeding time. Notched box-plots show the particle origin depth as a function of the seeding time (Figure 7). The increasing medians of the origin depth over time suggest that as the interbasin

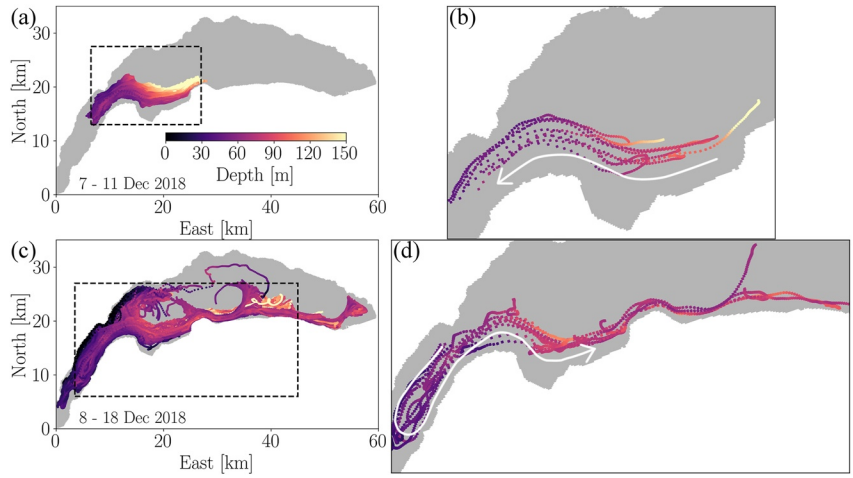

Figure 6. (a) Backward trajectories and (c) forward trajectories of particles released below 40-m depth in the *Petit Lac* hypolimnion (simulation B, red area Figure 1c). (b) and (d) Close-ups of the areas marked by the black dashed-lined rectangles in (a) and (c) showing backward and forward trajectories for a random subset of 10 particles, respectively. White arrows indicate the particle travel direction, that is, the movement of water parcels. The colorbar gives the particle depth. Only particles with an origin (backward tracking) and final (forward tracking) depth below 75 m are displayed.

upwelling advanced, *Grand Lac* water from progressively greater depths was transported into the *Petit Lac*. The increasing height of the boxes and the length of the whiskers with time and depth indicate that particles from a progressively wider depth range were drawn into the *Petit Lac*. This agrees with the continuously decreasing bottom temperatures observed at the confluence (Figures 2 and 3). Furthermore, the boxplots reveal that ~25% of the particles released on the last day of the upwelling phase originated from below 150-m depth. This is in good agreement with the estimated maximum origin depth of 180 m, based on lowest observed temperatures at MV-C (Figure 2e) and the full-depth profiles at SHL2 (Figure S5 in Supporting Information S1). Once upwelled into the *Petit Lac*, strong southwestward bottom currents transported these waters far into the *Petit Lac* along its thalweg, thus explaining the gradual thickening of its hypolimnion (Figures 4d and 5c, and Figure S10 in Supporting Information S1).

After the wind ceased and the currents reversed during the relaxation phase, the previously upwelled waters flowed back into the *Grand Lac* hypolimnion, as shown by the forward trajectories of simulation B (Figures 6c and 6d). Thus, the interbasin upwelling event effectively formed a current loop, that is, over the course of more than 1 week, hypolimnetic water from below 150-m depth first upwelled far into the *Petit Lac* and subsequently descended back into the *Grand Lac* hypolimnion mainly along the southern shore, confirming the field measurements (Figure 2). At the end of the forward tracking simulation on 18 December, that is, approximately 1 week after the last particles had been released, 78% of all particles were again found in the *Grand Lac* basin. The rest remained in the *Petit Lac* either because: (i) they had intruded too far toward the southwestern end of the lake to be affected by the outflow during the relaxation phase, or (ii) they were entrained into basin-scale gyres (Movie S1). This indicates that there was a significant net exchange of hypolimnetic water between the two basins during the interbasin upwelling event.

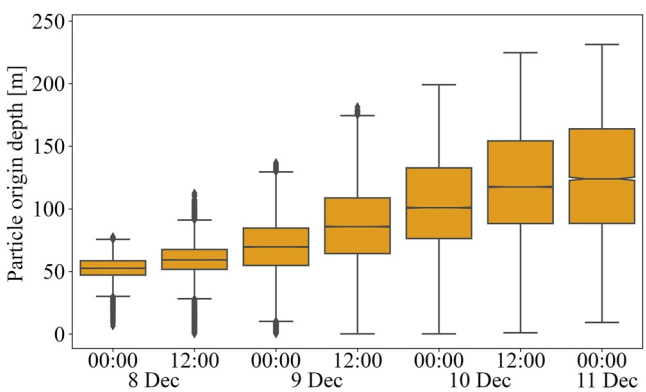

Figure 7. Notched box-plots of the particle origin depths during the upwelling phase obtained from the backward tracking results of simulation B as a function of the seeding time. The brown boxes give the interquartile range (first and third quartiles). The maximum length of the whiskers is 1.5 times the interquartile range and the diamonds mark the outliers. Dates refer to 2018.

To further analyze these current loops, ~200,000 particles were simultaneously released on 7 December at 13:00 below 50-m depth in the hypolimnion of the *Grand Lac* and forward tracked for ~10.5 days until 18 December at 00:00 (simulation L). Based on the backward tracking results of simulation B, the seeding locations and seeding time of simulation L were determined in such a way that all particles would upwell into the *Petit Lac* (blue area in Figure 1c; see Section 2.4 for details). For each particle, the maximum intrusion length into the *Petit Lac* was determined, and the time that each particle

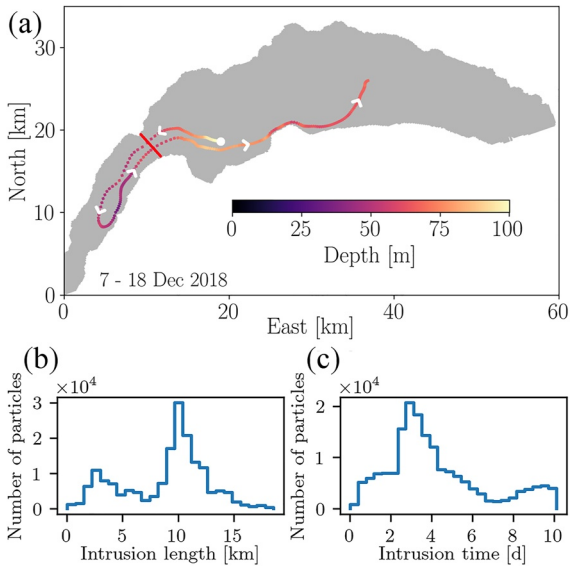

Figure 8. (a) Typical particle trajectory obtained from simulation L showing the complete current loop. The red line marks the confluence between the *Petit Lac* and *Grand Lac* and was used to calculate the intrusion length and time. The color bar gives the particle depth. The white circle marks the start of the trajectory with the white arrowheads indicating the travel direction. (b) and (c) Histograms of the intrusion length and time, respectively, obtained from simulation L.

spent in the *Petit Lac* before descending back into the *Grand Lac* was estimated (hereinafter referred to as intrusion time). A typical current loop trajectory, as well as the histograms of the intrusion length and time are shown in Figure 8.

Two peaks are evident in the intrusion length histogram (Figure 8b). The first one, at ∼3 km, represents a small portion of the particles that did not intrude significantly into the *Petit Lac*. They were immediately upwelled into its epilimnion and consequently flushed out back into the *Grand Lac* by the strong surface outflow. The second and more prominent peak shows that the majority of the particles intruded ∼10 km or more into the *Petit Lac* (Figure 8b), that is, approximately half its total length. Furthermore, these particles spent on average 3–4 days in the shallow basin before being flushed out again (Figure 8c). The small peak between 8 and 10 days and the sharp cut-off at the end of the time axis of the intrusion time histogram represent the fraction of the upwelled particles that had not left the *Petit Lac* by the end of the simulation.

Out of all the forward-tracked particles of simulation B that returned to the *Grand Lac*, 70% reached a maximum depth greater than 75 m, that is, lower than the maximum depth of the *Petit Lac*, and 20%, greater than 100 m (Figure S11 in Supporting Information S1). Subject to the Coriolis force, the outflowing deep-reaching particles predominantly followed the southern shore of the *Grand Lac*, forming a strong shore-hugging current that reached the eastern end of Lake Geneva by the end of the simulation, traveling a distance of ∼50 km (Figure 6c). The presence of this eastward narrow jet during the relaxation phase was confirmed by ADCP measurements at 100 and 150-m depth near the southern shore of the *Grand Lac* in December 2019 (Figure S12 in Supporting Information S1). A significant number of these particles was entrained into basin-scale gyres and subsequently spread over large parts of the *Grand Lac* hypolimnion (Figures 6c and 6d). A similar trapping and horizontal redistribution of water masses within gyres in Lake Geneva was reported by Cimatoribus et al. (2019) and Reiss et al. (2020).

During both the upwelling and relaxation phases, a two-layer current structure with opposing current directions in the epilimnion and hypolimnion of the *Petit Lac* prevailed, resulting in large vertical shear (Figures 2 and 4). Furthermore, the moored ADCP measurements showed counterflowing bottom currents at the northern (MV-N) and southern (MV-S) sections of the confluence during both periods, suggesting enhanced horizontal shear (Figure 2). Considering this enhanced horizontal and vertical shear and the relatively low stability of the water column during winter, turbulent mixing between the upwelled *Grand Lac* and surrounding *Petit Lac* waters can be expected. Gradient Richardson numbers (*Ri*) in the *Petit Lac* were computed from the modeled velocity and temperature field and are given for selected vertical transects during the upwelling phase on 9 December 2018 at 14:00 in Figure S13 in Supporting Information S1. Low *Ri* values are observed both near the bottom and at the northern shore, indicating turbulent mixing between the upwelled and ambient waters. Furthermore, significant temperature inversions in the hypolimnion and around the thermocline depth seen in the CTD transects taken on 13 December 2018 at ∼11:00 at different locations in the *Petit Lac* suggest active overturning and hence mixing (Figures S1c and S1d in Supporting Information S1). The time evolution of *Ri* during the entire interbasin upwelling event is shown in Movie S1.

The particle tracking results of simulations B and L confirm that during the interbasin upwelling event investigated, there was a net exchange of hypolimnetic water between the two basins. The resulting current loop may thus be an important transport process for interbasin exchange and an efficient mechanism for advective vertical exchange within the hypolimnion of Lake Geneva. The results also show that turbulent mixing between the upwelled and ambient waters due to strong vertical and horizontal shear appears to occur during the entire interbasin upwelling event. Since water quality in the *Petit Lac* is better than that of the deep hypolimnion of the *Grand Lac* (CIPEL, 2016), the enhanced hypolimnetic exchange and mixing between the two basins induced by this regularly occurring wind-induced transport process can be regarded as ecologically beneficial.

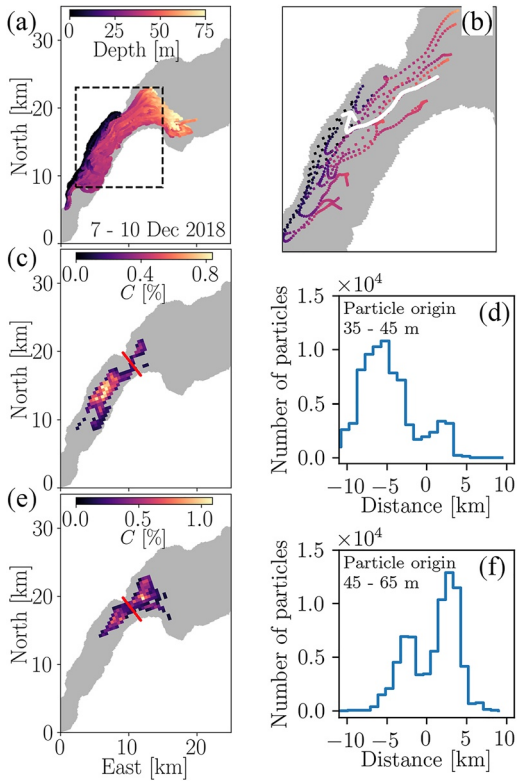

Figure 9. (a) Backward trajectories of particles released between 0- to 15-m depth near the northern shore of the *Petit Lac* basin (simulation S; green area in Figure 1c). (b) Close-up of selected backward trajectories. The colorbar in (a) gives the particle depth. Only particles originating from below 35-m depth are displayed. The white arrow indicates the travel direction. (c) and (e) 2D maps of origin locations of particles originating from 35- to 45-m and 45- to 65-m depths, respectively, as inferred from the backward tracking simulation S. (d) and (f) Histograms of the distance from the particle origin to the confluence (red lines in c and e), corresponding to the depth ranges in (c) and (e), respectively. Positive values indicate particles originating from the *Grand Lac*. The colorbars in (c) and (e) show the particle concentrations as percentages, that is, the depth-accumulated number of particles per horizontal cell divided by the total number of particles originating from below 35-m depth. Each horizontal cell is composed of 16 binned model grid cells, that is, 4×113 m by 4×113 m. For clarity, binned cells with less than 150 particles ($C \leq 0.1\%$) are not shown.

In late winter, that is, from mid-January to March 2019, when the thermocline was below the maximum depth at the confluence and the *Petit Lac* was fully mixed, no deep interbasin upwelling was observed under comparably strong *Vent* wind conditions (not shown here). This suggests that stratification in the *Petit Lac* is necessary for this upwelling to occur, because the observed two-layer current structure is imposed by the presence of a thermocline in the shallow basin, in agreement with the findings on hypolimnetic exchange between Lake Erie's deep eastern and shallow central basins (Bartish, 1987).

3.3.2. Coastal Upwelling at the Northern Shore of the *Petit Lac*: Origin and Dynamics

Some particles, especially those seeded at earlier times and at shallower depths, were entrained by coastal upwelling currents and transported into the epilimnion along the northern shore of the *Petit Lac*, in agreement with the lower surface temperatures observed in the model results in that area (Figure 4a). To address this coastal upwelling, backward tracking was used to determine the origin of particles released during the upwelling phase between 0- and 15-m depth near the northern shore of the *Petit Lac* (simulation S, green area in Figure 1c). The corresponding particle trajectories of subsets of ~2,500 and 10 particles are shown in Figure 9a and 9b, respectively. Approximately 50% of all particles originated from the epilimnion, that is, between 0- and 35-m depth. The remaining half came from 35- to 65-m depth, that is, from within the hypolimnion, thus confirming that the lower surface temperatures observed in the model results were due to coastal upwelling of hypolimnetic water (Figure 4a).

A further breakdown of the particle origin locations shows that approximately half of all coastally upwelled particles originating from the hypolimnion came from depths of 35–45 m, and the other half came from depths of 45 to 65 m. Figure 9 depicts the origin locations for both groups of particles in the form of 2D concentration maps and histograms of the distance from the particle origin to the confluence. The majority of the particles that originated from just below the thermocline, that is, 35- to 45-m depth, came from within the *Petit Lac* (Figures 9c and 9d). On the other hand, the bulk of the particles that upwelled from below 45-m depth came from the *Grand Lac*. This can be readily explained by the strong southwestward bottom currents in the *Petit Lac* (Figures 9e and 9f). Before actually upwelling into the epilimnion, these hypolimnetic particles traveled southwestward along the main axis of the *Petit Lac* for several kilometers, following the strong bottom currents (Figure 9b). With a typical velocity of the bottom currents of 20 cm s^{-1} and a length scale of 3 km (minimum intrusion length into the *Petit Lac* before upwelling; Figure 10c), a Rossby number of ~0.6, that is, <1 is obtained, indicating that Coriolis force is important.

Once upwelled into the surface layers, the cold waters were advected downwind along the shore (e.g., Figure 9b). The exact upwelling location of each particle was used to retrace the upwelling motions and pinpoint hotspots along the shoreline where coastal upwelling was most likely to occur. This was achieved by finding the time and location where each particle initially rose and then stayed above 25-m depth for at least 4 hr. Three trajectory examples with the upwelling location determined accordingly are given in Figure 10a. The corresponding concentration maps of the upwelling locations for all particles coming from 35- to 45-m and 45- to 65-m depths are shown in Figures 10b and 10c, respectively. The spatial patterns of the upwelling locations are significantly different for the two groups.

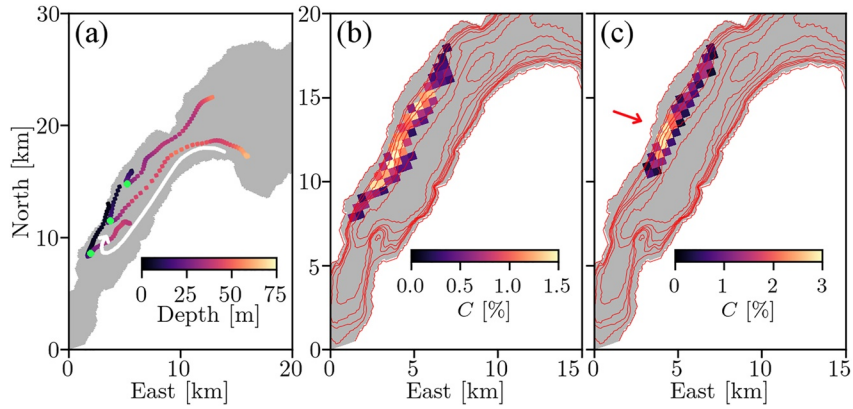

Figure 10. (a) Examples of particle trajectories that upwelled at the northern shore of the *Petit Lac* basin with the estimated upwelling locations marked by the green dots. The colorbar gives the particle depth. The white arrow indicates the travel direction. (b) and (c) 2D concentration maps of the upwelling locations for particles originating from 35- to 45-m and 45- to 65-m depths, respectively, as inferred from backward tracking simulation S. The overlaid red contours show the isobaths between 0- and 70-m depth at 10 m intervals. The colorbars in (b) and (c) indicate the upwelling occurrence as percentages, that is, the number of upwelled particles per horizontal cell divided by the total number of particles originating from the considered depth range. Each horizontal cell is composed of 16 binned model grid cells, that is, 4 × 113 m by 4 × 113 m. For clarity, binned cells with less than 380 particles ($C \leq 0.25\%$) are not shown.

While the coastal upwelling from 35- to 45-m depth, that is, just below the thermocline, was relatively uniform over a 1-km × 8-km wide area (Figure 10b), the upwelling from deeper within the hypolimnion was more localized. In particular, upwelling appeared to be focused in an area ∼7 km southwest of the confluence (red arrow in Figure 10c). The overlaid isobaths in Figure 10c indicate that this location coincided with a region where the isobaths between 50- to 60-m depth stretched in the cross-shore direction and, conversely, the slope between 40- and 50-m depth steepens. The observed upwelling hotspot can be explained by the combined effects of: (a) the shoreward Coriolis deflection of the southwestward bottom currents and (b) the shoreward-veering 50-m isobath, which favors the onshore deflection of the bottom currents and thus locally enhances the coastal upwelling.

The subsequent fate of the particles released in the upper 15 m of the *Petit Lac* during the upwelling phase was determined by forward tracking. At the end of the simulation on 18 December, 70% of all particles had been flushed back into the *Grand Lac*. Nearly all of these particles descended below 40-m depth, that is, into the hypolimnion, with 16% of them descending temporarily to depths between 75 and 100 m. Furthermore, the particles reaching the *Grand Lac* hypolimnion accumulated along the southern shore at the end of simulation S (Figure S14 in Supporting Information S1), indicating that they were entrained into the eastward shore-hugging current discussed above (Figures 6c and 6d).

3.4. Interbasin Upwelling: A Mechanism Contributing to Deepwater Renewal

Thus far, we have detailed one *Vent* wind-induced interbasin upwelling event and the accompanying coastal upwelling in the *Petit Lac* that took place in mid-December 2018. However, *Vent* winds are the most frequent strong winter winds in the region (e.g., CH2018, 2018), suggesting that this process occurs regularly and therefore could have an important impact on the deepwater dynamics in Lake Geneva.

Three other comparable interbasin upwelling events occurred between October 2018 and January 2019, that is, when the *Petit Lac* was weakly stratified. Figure 11 shows the corresponding modeled current velocities and depth-averaged near-bottom temperatures at the northern confluence (see Figure 1a for location), as well as the spatially-averaged wind speeds over western Lake Geneva derived from COSMO-1 data. Observational data for these events are given in Figure S2 in Supporting Information S1. Furthermore, particle tracking simulations similar to simulation B (see Section 3.3.1) were run, with particles released every 2 hr in the *Petit Lac* hypolimnion (Figure 1c) during the last 24 hr of each upwelling event and tracked backward to its beginning. The results show that during each event, *Grand Lac* waters from as deep as ∼150-m depth were upwelled into the

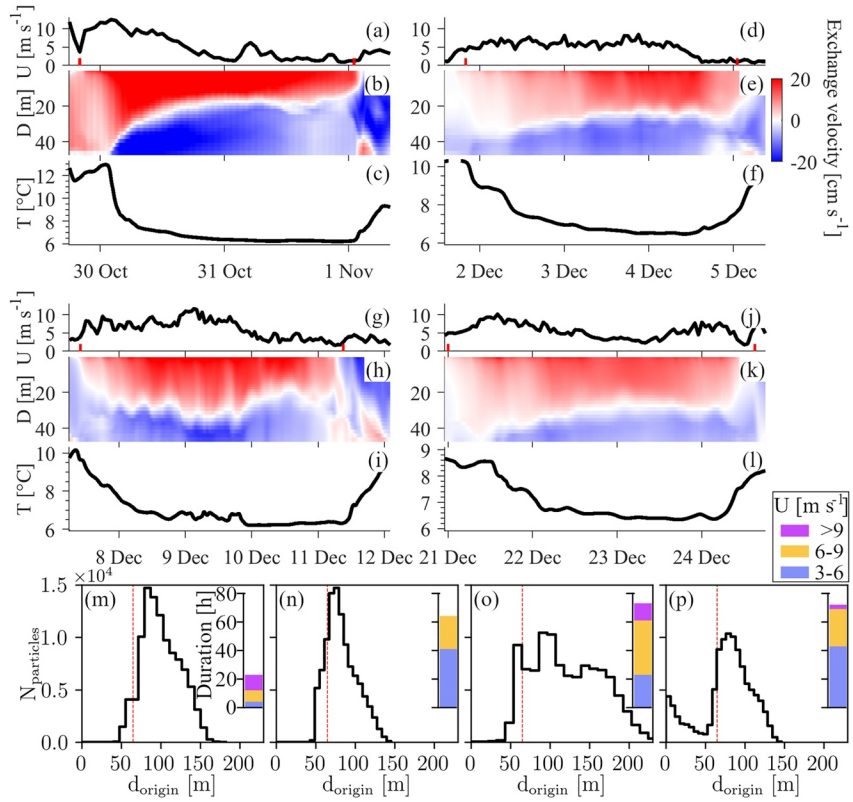

Figure 11. Wind speed (a, d, g, j), modeled interbasin exchange velocity (b, e, h, k), and depth-averaged temperature in the lowest 10 m of the water column (c, f, i, l) at mooring MV-N (see Figure 1b for location), for each of the four interbasin upwelling events between October and December 2018. Histograms of particle origin depths for each event are given in chronological order in panels (m) to (p) (details in Section 3.4), with the inset stacked bar charts showing the corresponding *Vent* wind speeds and duration. All wind speeds are based on COSMO-1 data and were spatially-averaged over the *Petit Lac* and the western *Grand Lac* basins (~6 km into the *Grand Lac* from the confluence). For the bar charts, only *Vent* winds from the south-west sector, that is, 180°–270°, and wind speeds >3 m s^{-1} were considered, with the red ticks in the wind time series plots (a, d, g, j) marking the corresponding time period that was considered. The vertical red dashed line in panels (m) to (p) shows the maximum depth at the confluence.

shallow basin (Figures 11m–11p), corresponding to vertical excursions of O(100 m). It is important to note that the *Vent* wind-induced interbasin upwelling studied here is completely different than the interbasin exchange due to internal Kelvin waves discussed by Umlauf and Lemmin (2005). Internal Kelvin waves, which are shore-hugging, can induce comparably strong current velocities and a comparable volume exchange between the two basins. However, since the exchange is predominantly horizontal, it cannot produce upwelling of deep hypolimnetic waters from the *Grand Lac* into the *Petit Lac* basin.

Although the mid-December 2018 event discussed above had the most pronounced upwelling (from ~200-m depth; Figure 11o), the wind stress during that event was not particularly strong or enduring for a wintertime *Vent* wind, and 2018 was not an exceptionally windy year (see wind data from 1981 to 2021 in Figure S15 in Supporting Information S1). This indicates that interbasin upwelling events of similar magnitude occur regularly. Considering the deep origins of the upwelled waters, the great intrusion lengths and times, and the enhanced mixing by shear between inflowing and outflowing water masses, our findings suggest that interbasin upwelling occurs frequently and can be an important mechanism for deepwater renewal and horizontal and vertical nutrient recycling in Lake Geneva.

This study focused on *Vent* wind-induced interbasin exchange. However, at the same time, *Vent* winds also produce coastal upwelling of hypolimnetic waters from ~150- to 200-m depth at the northern *Grand Lac* shore (Reiss et al., 2020), further corroborating the overall importance of these winds in driving the dynamics in the deep hypolimnion and contributing to deepwater renewal in Lake Geneva. The latter agrees with long-term

observational data at CIPEL station SHL2 that shows an increase in dissolved oxygen levels at ~300-m depth every winter, even during mild winters with incomplete convective overturning (e.g., figure 26 in CIPEL, 2016; Lemmin, 2020). The *Vent* wind-induced interbasin upwelling discussed here can therefore be considered as a newly identified piece in the puzzle of Lake Geneva's deepwater renewal dynamics, which appear to be strongly influenced by 3D transport processes (Lemmin, 2020). Further studies are required to quantify the relative contribution of the aforementioned upwelling processes, as well as other transport processes, such as cold-water density currents due to differential cooling (Fer et al., 2002; Lemmin, 2020). Budgets of numerical tracers offer a promising approach for addressing this question (e.g., Matsumoto et al., 2015; Umlauf & Lemmin, 2005).

4. Summary and Conclusions

Combining field observations, 3D hydrodynamic modeling and particle tracking, we investigated in detail wind-driven interbasin exchange, and in particular hypolimnetic upwelling, between the deep *Grand Lac* (max. depth 309 m) and shallow *Petit Lac* (max. depth 75 m) basins of Lake Geneva during the weakly stratified winter period. Although this process has thus far received little attention, our results suggest that it could play an increasingly important role in deepwater renewal in the future as convective cooling continues to weaken due to global warming.

We demonstrated that *Vent* winds from the southwest effectively create a current loop whereby waters from the deep *Grand Lac* hypolimnion are drawn into the shallower *Petit Lac*. Once upwelled, these waters are advected far into the *Petit Lac*, doubling its hypolimnion volume. After the wind ceased, they drained back into the *Grand Lac* hypolimnion, where they spread horizontally over a large area, with parts entrained into gyres. An in-depth analysis of one such event in mid-December 2018 revealed that Coriolis force strongly modified the circulation and the trajectories of the water masses.

During the interbasin upwelling, hypolimnetic *Grand Lac* water originating from below 150-m depth remained ~3–4 days in the *Petit Lac,* and was thus brought into prolonged contact with "fresher" (i.e., better quality) *Petit Lac* water. Furthermore, strong shear between the inflowing hypolimnion waters and the outflowing epilimnion waters and a relatively weak stratification favored turbulent mixing between these different waters, as suggested by low, model-based gradient Richardson numbers and temperature inversions measured near the bottom and around the thermocline.

At the same time that deep upwelling took place in the *Petit Lac* hypolimnion, coastal upwelling occurred at its northern shore. Particle tracking revealed that waters from ~65-m depth in the *Grand Lac* hypolimnion were first drawn into the *Petit Lac* hypolimnion and subsequently upwelled at its northern shore, which enhanced hypolimnetic-epilimnetic exchange and mixing, and thus further contributed to the renewal of *Grand Lac* hypolimnetic waters.

Since *Vent* winds are the most frequent strong winter winds over Lake Geneva and last for days, this deepwater upwelling process occurs several times every winter. Altogether, our findings confirm that wind-driven interbasin upwelling in Lake Geneva is potentially an important, yet thus far overlooked, transport process for deepwater renewal, deep ventilation, and nutrient cycling. If in the future, the *Petit Lac* basin remains stratified over a longer period due to global warming, then the time window during which interbasin upwelling can occur will be extended, thus further enhancing the overall importance of this process.

Due to its strongly transient and three-dimensional nature, interbasin upwelling cannot be adequately described by traditional one-dimensional (1D) concepts. This process can also occur in other deep multi-basin lakes under similar conditions. Unlike convective winter cooling, it is less susceptible to global warming. The findings of this study should be taken into consideration when establishing long-term predictions of lake system dynamics related to climate change.

Data Availability Statement

The in situ data and model results supporting the findings of this study are available online at https://doi.org/10.5281/zenodo.6564426.

Acknowledgments
This work was supported by the Swiss National Science Foundation (Grant No. 159422) and the Bois Chamblard Foundation, https://www.bois-chamblard.ch/en/ (last accessed on 3 June 2021). Meteorological data were provided by the Federal Office of Meteorology and Climatology in Switzerland (MeteoSwiss, last accessed on 3 June 2021). Full-depth temperature profile data at CIPEL station SHL2 were provided by © OLA-IS, AnaEE-France, INRAE of Thonon-les-Bains, CIPEL (Rimet et al., 2020). Temperature profile data at CIPEL station GE3 were provided by the Service de l'Ecologie de l'Eau (Département du territoire, Office cantonal de l'eau, SECOE, 1211 Genève, Suisse, https://www.ge.ch/organisation/oceau-service-ecologie-eau, last accessed on 3 June 2021). We thank Htet Kyi Wynn and Benjamin Graf for assisting with the fieldwork. We thank the three anonymous reviewers for their constructive comments and suggestions that helped improve the manuscript. Open access funding provided by Ecole Polytechnique Federale de Lausanne.

References

Aeschbach-Hertig, W., Kipfer, R., Hofer, M., Imboden, D. M., & Baur, H. (1996). Density-driven exchange between the basins of Lake Lucerne (Switzerland) traced with the ^{3}H-^{3}He method. *Limnology & Oceanography*, *41*, 707–721. https://doi.org/10.4319/lo.1996.41.4.0707

Ahrnsbrak, W. F., & Wing, M. R. (1998). Wind-induced hypolimnion exchange in Lake Ontario's Kingston basin: Potential effects on oxygen. *Journal of Great Lakes Research*, *24*, 145–151. https://doi.org/10.1016/S0380-1330(98)70806-8

Amadori, M., Piccolroaz, S., Dijkstra, H. A., & Toffolon, M. (2020). What makes an elongated lake "large"? Scales from wind-driven steady circulation on a rotating Earth. *Journal of Great Lakes Research*, *46*, 703–717. https://doi.org/10.1016/j.jglr.2019.10.013

Amadori, M., Piccolroaz, S., Giovannini, L., Zardi, D., & Toffolon, M. (2018). Wind variability and Earth's rotation as drivers of transport in a deep, elongated subalpine lake: The case of Lake Garda. *Journal of Limnology*, *77*, 505–521. https://doi.org/10.4081/jlimnol.2018.1814

Appt, J., Imberger, J., & Kobus, H. (2004). Basin-scale motion in stratified Upper Lake Constance. *Limnology & Oceanography*, *49*, 919–933. https://doi.org/10.4319/lo.2004.49.4.0919

Bartish, T. (1987). A review of exchange processes among the three basins of Lake Erie. *Journal of Great Lakes Research*, *13*, 607–618. https://doi.org/10.1016/S0380-1330(87)71676-1

Bauer, S. W., Graf, W. H., Mortimer, C. H., & Perrinjaquet, C. (1981). Inertial motion in Lake Geneva (Le Léman). *Archives for Meteorology, Geophysics, and Bioclimatology, Series A*, *30*, 289–312. https://doi.org/10.1007/BF02257850

Bennett, E. B. (1988). On the physical limnology of Georgian Bay. In M. Munawar (Ed.), *Limnology and fisheries of Georgian Bay and the north channel ecosystems*. Springer. (pp. 21–34). Last accessed 3 June 2021. Received from https://www.springer.com/gp/book/9789061936534

Bouffard, D., & Lemmin, U. (2013). Kelvin waves in Lake Geneva. *Journal of Great Lakes Research*, *39*, 637–645. https://doi.org/10.1016/j.jglr.2013.09.005

Boyce, F. M., Chiocchio, F., Eid, B., Penicka, F., & Rosa, F. (1980). Hypolimnion flow between the central and eastern basins of Lake Erie during 1977 (Interbasin hypolimnion flows). *Journal of Great Lakes Research*, *6*, 290–306. https://doi.org/10.1016/S0380-1330(80)72110-X

CH2018. (2018). CH2018 – Climate scenarios for Switzerland, technical report, National Centre for Climate services. p. 271. ISBN: 978-3-9525031-4-0. Last accessed 3 June 2021. Retrieved from https://naturalsciences.ch/service/publications/107865-ch2018--climate-scenarios-for-switzerland-technical-report

Cimatoribus, A. A. (2018). *C-tracker*. https://doi.org/10.5281/zenodo.1034118

Cimatoribus, A. A., Lemmin, U., & Barry, D. A. (2019). Tracking Lagrangian transport in Lake Geneva: A 3D numerical modeling investigation. *Limnology & Oceanography*, *64*, 1–18. https://doi.org/10.1002/lno.11111

Cimatoribus, A. A., Lemmin, U., Bouffard, D., & Barry, D. A. (2018). Nonlinear dynamics of the nearshore boundary layer of a large lake (Lake Geneva). *Journal of Geophysical Research: Oceans*, *123*, 1016–1031. https://doi.org/10.1002/2017JC013531

CIPEL. (2016). *Rapports sur les études et recherches entreprises dans le bassin lémanique, Campagne 2015*. Commission internationale pour la protection des eaux du Léman (CIPEL). Last accessed 30 May 2022. Retrieved from https://www.cipel.org/wp-content/uploads/2021/06/rapportscientifique-camp-2015-vf.pdf

CIPEL. (2019). *Rapports sur les études et recherches entreprises dans le bassin lémanique, Campagne 2018*. Commission internationale pour la protection des eaux du Léman (CIPEL). Last accessed 30 May 2022. Retrieved from https://www.cipel.org/wp-content/uploads/2021/06/rapportscientifique-camp-2018-vf.pdf

Coman, M. A., & Wells, M. G. (2012). Temperature variability in the nearshore benthic boundary layer of Lake Opeongo is due to wind-driven upwelling events. *Canadian Journal of Fisheries and Aquatic Sciences*, *69*, 282–296. https://doi.org/10.1139/f2011-167

Cornett, R., & Rigler, F. (1979). Hypolimnetic oxygen deficits: Their prediction and interpretation. *Science*, *205*, 580–581. https://doi.org/10.1126/science.205.4406.580

Djoumna, G., Lamb, K. G., & Rao, Y. R. (2014). Sensitivity of the parameterizations of vertical mixing and radiative heat fluxes on the seasonal evolution of the thermal structure of Lake Erie. *Atmosphere-Ocean*, *52*, 294–313. https://doi.org/10.1080/07055900.2014.939824

Döös, K., Kjellsson, J., & Jönsson, B. (2013). TRACMASS—a Lagrangian trajectory model. In T. Soomere, & E. Quak (Eds.), *Preventive methods for coastal protection: Towards the use of ocean dynamics for pollution control* (pp. 225–249). Springer. Last accessed 3 June 2021. Retrieved from https://www.springerprofessional.de/en/tracmass-a-lagrangian-trajectory-model/1994902

Dorostkar, A., & Boegman, L. (2013). Internal hydraulic jumps in a long narrow lake. *Limnology & Oceanography*, *58*, 153–172. https://doi.org/10.4319/lo.2013.58.1.0153

Dorostkar, A., Boegman, L., & Pollard, A. (2017). Three-dimensional simulation of high-frequency nonlinear internal wave dynamics in Cayuga Lake. *Journal of Geophysical Research: Oceans*, *122*, 2183–2204. https://doi.org/10.1002/2016JC011862

Fer, I., Lemmin, U., & Thorpe, S. A. (2002). Winter cascading of cold water in Lake Geneva. *Journal of Geophysical Research*, *107*, 13–16. https://doi.org/10.1029/2001JC000828

Flood, B., Wells, M., Dunlop, E., & Young, J. (2020). Internal waves pump waters in and out of a deep coastal embayment of a large lake. *Limnology & Oceanography*, *65*, 205–223. https://doi.org/10.1002/lno.11292

Goldman, C. R., Kumagai, M., & Robarts, R. D. (Eds.) (2013). *Climatic change and global warming of inland waters: Impacts and mitigation for ecosystems and societies*. Wiley-Blackwell. https://doi.org/10.1002/9781118470596

Graf, W. H., & Prost, J. P. (1980). Aerodynamic drag and its relation to the sea state: With data from Lake Geneva. *Archiv für Meteorologie, Geophysik und Bioklimatologie, Serie A*, *29*, 67–87. https://doi.org/10.1007/BF02247734

Hamze-Ziabari, S. M., Razmi, A. M., Lemmin, U., & Barry, D. A. (2022). Detecting submesoscale cold filaments in a basin-scale gyre in large, deep Lake Geneva (Switzerland/France). *Geophysical Research Letters*, *49*, e2021GL096185. https://doi.org/10.1029/2021GL096185

Jabbari, A., Ackerman, J. D., Boegman, L., & Zhao, Y. (2019). Episodic hypoxia in the western basin of Lake Erie. *Limnology & Oceanography*, *64*, 2220–2236. https://doi.org/10.1002/lno.11180

Jabbari, A., Ackerman, J. D., Boegman, L., & Zhao, Y. (2021). Increases in Great Lake winds and extreme events facilitate interbasin coupling and reduce water quality in Lake Erie. *Scientific Reports*, *11*, 5733. https://doi.org/10.1038/s41598-021-84961-9

Kocsis, O., Mathis, B., Gloor, M., Schurter, M., & Wüest, A. (1998). Enhanced mixing in narrows: A case study at the Mainau sill (Lake Constance). *Aquatic Sciences*, *60*, 236. https://doi.org/10.1007/s000270050039

Laval, B. E., Morrison, J., Potts, D. J., Carmack, E. C., Vagle, S., James, C., et al. (2008). Wind-driven summertime upwelling in a fjord-type lake and its impact on downstream river conditions: Quesnel Lake and River, British Columbia, Canada. *Journal of Great Lakes Research*, *34*, 189–203. https://doi.org/10.3394/0380-1330(2008)34[189:WSUIAF]2.0.CO;2

Lavigne, S., & Nirel, P. (2016). *Physico-chemical and biological changes in the waters of the Petit Lac*. Service de l'écologie de l'eau (SECOE). Last accessed 30 May 2022. Retrieved from https://www.cipel.org/wp-content/uploads/catalogue/0-evolution-physico-chimique-biologique-petit-lac-camp-2015.pdf

Lawrence, G. A., Burke, J. M., Murphy, T. P., & Prepas, E. E. (1997). Exchange of water and oxygen between the two basins of Amisk Lake. *Canadian Journal of Fisheries and Aquatic Sciences*, *54*, 2121–2132. https://doi.org/10.1139/f97-235

Lemmin, U. (2020). Insights into the dynamics of the deep hypolimnion of Lake Geneva as revealed by long-term temperature, oxygen, and current measurements. *Limnology & Oceanography*, *65*, 2092–2107. https://doi.org/10.1002/lno.11441

Lemmin, U., & D'Adamo, N. (1996). Summertime winds and direct cyclonic circulation: Observations from Lake Geneva. *Annales Geophysicae*, *14*, 1207–1220. https://doi.org/10.1007/s00585-996-1207-z

Lemmin, U., Mortimer, C. H., & Bäuerle, E. (2005). Internal seiche dynamics in Lake Geneva. *Limnology & Oceanography*, *50*, 207–216. https://doi.org/10.4319/lo.2005.50.1.0207

Marshall, J., Adcroft, A., Hill, C., Perelman, L., & Heisey, C. (1997). A finite-volume, incompressible Navier Stokes model for studies of the ocean on parallel computers. *Journal of Geophysical Research*, *102*, 5753–5766. https://doi.org/10.1029/96JC02775

Matsumoto, K., Tokos, K. S., & Gregory, C. (2015). Ventilation and dissolved oxygen cycle in Lake Superior: Insights from a numerical model. *Geochemistry, Geophysics, Geosystems*, *16*, 3097–3110. https://doi.org/10.1002/2015GC005916

Monismith, S. G., Imberger, J., & Morison, M. L. (1990). Convective motions in the sidearm of a small reservoir. *Limnology & Oceanography*, *35*, 1676–1702. https://doi.org/10.4319/lo.1990.35.8.1676

Monsen, N. E., Cloern, J. E., Lucas, L. V., & Monismith, S. G. (2002). A comment on the use of flushing time, residence time, and age as transport time scales. *Limnology & Oceanography*, *47*, 1545–1553. https://doi.org/10.4319/lo.2002.47.5.1545

Nguyen, T. D., Thupaki, P., Anderson, E. J., & Phanikumar, M. S. (2014). Summer circulation and exchange in the Saginaw Bay-Lake Huron system. *Journal of Geophysical Research: Oceans*, *119*, 2713–2734. https://doi.org/10.1002/2014JC009828

Niu, Q., Xia, M., Rutherford, E. S., Mason, D. M., Anderson, E. J., & Schwab, D. J. (2015). Investigation of interbasin exchange and interannual variability in Lake Erie using an unstructured-grid hydrodynamic model. *Journal of Geophysical Research: Oceans*, *120*, 2212–2232. https://doi.org/10.1002/2014JC010457

Nürnberg, G. K., Molot, L. A., O'Connor, E., Jarjanazi, H., Winter, J., & Young, J. (2013). Evidence for internal phosphorus loading, hypoxia and effects on phytoplankton in partially polymictic Lake Simcoe, Ontario. *Journal of Great Lakes Research*, *39*, 259–270. https://doi.org/10.1016/j.jglr.2013.03.016

Okubo, K. (1995). Field observations of the dense bottom current between the north and south basins. In S. Okuda, J. Imberger, & M. Kumagai (Eds.), *Physical processes in a large lake: Lake Biwa, Japan* (Vol. 48, pp. 43–51). American Geophysical Union. *Coastal and Estuarine Studies Series*. https://doi.org/10.1029/CE048p0043

Oonishi, Y. (1995). Numerical simulation of density-induced currents between the north and south basins of Lake Biwa. In S. Okuda, J. Imberger, & M. Kumagai (Eds.), *Physical processes in a large lake: Lake Biwa, Japan* (Vol. 48, pp. 53–64). American Geophysical Union. *Coastal and Estuarine Studies Series*. https://doi.org/10.1029/CE048p0053

Piccolroaz, S., Amadori, M., Toffolon, M., & Dijkstra, H. A. (2019). Importance of planetary rotation for ventilation processes in deep elongated lakes: Evidence from Lake Garda (Italy). *Scientific Reports*, *9*, 8290. https://doi.org/10.1038/s41598-019-44730-1

Pöschke, F., Lewandowski, J., Engelhardt, C., Preuß, K., Oczipka, M., Ruhtz, T., & Kirillin, G. (2015). Upwelling of deep water during thermal stratification onset—a major mechanism of vertical transport in small temperate lakes in spring? *Water Resources Research*, *51*, 9612–9627. https://doi.org/10.1002/2015WR017579

Rao, Y. R., & Murthy, C. R. (2001). Nearshore currents and turbulent exchange processes during upwelling and downwelling events in Lake Ontario. *Journal of Geophysical Research*, *106*, 2667–2678. https://doi.org/10.1029/2000JC900149

Reiss, R. S., Lemmin, U., Cimatoribus, A. A., & Barry, D. A. (2020). Wintertime coastal upwelling in Lake Geneva: An efficient transport process for deepwater renewal in a large, deep lake. *Journal of Geophysical Research: Oceans*, *125*, e2020JC016095. https://doi.org/10.1029/2020JC016095

Rimet, F., Anneville, O., Barbet, D., Chardon, C., Crépin, L., Domaizon, I., et al. (2020). The Observatory on LAkes (OLA) database: Sixty years of environmental data accessible to the public: The Observatory on LAkes (OLA) database. *Journal of Limnology*, *79*, 164–178. https://doi.org/10.4081/jlimnol.2020.1944

Roberts, D. C., Egan, G. C., Forrest, A. L., Largier, J. L., Bombardelli, F. A., Laval, B. E., et al. (2021). The setup and relaxation of spring upwelling in a deep, rotationally influenced lake. *Limnology & Oceanography*, *66*, 1168–1189. https://doi.org/10.1002/lno.11673

Salmaso, N. (2005). Effects of climatic fluctuations and vertical mixing on the interannual trophic variability of Lake Garda, Italy. *Limnology & Oceanography*, *50*, 553–565. https://doi.org/10.4319/lo.2005.50.2.0553

Saylor, J. H., & Miller, G. S. (1987). Studies of large-scale currents in Lake Erie, 1979–80. *Journal of Great Lakes Research*, *13*, 487–514. https://doi.org/10.1016/S0380-1330(87)71668-2

Scavia, D., Allan, J. D., Arend, K. K., Bartell, S., Beletsky, D., Bosch, N. S., et al. (2014). Assessing and addressing the re-eutrophication of Lake Erie: Central basin hypoxia. *Journal of Great Lakes Research*, *40*, 226–246. https://doi.org/10.1016/j.jglr.2014.02.004

Soulignac, F., Lemmin, U., Ziabari, S. M. H., Wynn, H. K., Graf, B., & Barry, D. A. (2021). Rapid changes in river plume dynamics caused by advected wind-driven coastal upwelling as observed in Lake Geneva. *Limnology & Oceanography*, *66*, 3116–3133. https://doi.org/10.1002/lno.11864

Umlauf, L., & Lemmin, U. (2005). Interbasin exchange and mixing in the hypolimnion of a large lake: The role of long internal waves. *Limnology & Oceanography*, *50*, 1601–1611. https://doi.org/10.4319/lo.2005.50.5.1601

van Senden, D. C., & Imboden, D. M. (1989). Internal seiche pumping between sill-separated basins. *Geophysical & Astrophysical Fluid Dynamics*, *48*, 135–150. https://doi.org/10.1080/03091928908219530

Voudouri, A., Avgoustoglou, E., & Kaufmann, P. (2017). Impacts of observational data assimilation on operational forecasts. Springer International Publishing. In T. Karacostas, A. Bais, & P. Nastos (Eds.), *Perspectives on atmospheric sciences* (pp. 143–149). https://doi.org/10.1007/978-3-319-35095-0

Wells, M. G., & Sealock, L. (2009). Summer water circulation in Frenchman's Bay, a shallow coastal embayment connected to Lake Ontario. *Journal of Great Lakes Research*, *35*, 548–559. https://doi.org/10.1016/j.jglr.2009.08.009